Vertical wave packets observed in a crystallized hexagonal monolayer complex plasma

D. Samsonov, S. Zhdanov,* and G. Morfill
Max-Planck-Institut für Extraterrestrische Physik, D-85740 Garching, Germany
(Received 30 January 2004; revised manuscript received 27 May 2004; published 24 February 2005)

Propagation of vertical wave packets was observed experimentally in a crystallized hexagonal monolayer complex plasma. It was found that the phase velocity exceeded the group velocity by a factor 65 and was directed into the opposite direction as expected for an inverse optical-like dispersion relation. The wave packets propagated keeping their width constant. The explanation of this behavior is based on three-dimensional equations of motion and uses a long-wavelength weak dispersion weak inhomogeneity approximation. While the wave dispersion causes the wave packet to spread, lattice inhomogeneity and neutral gas drag counteract spreading. A plasma diagnostic method was developed that is based on the ratio between vertical and dust-lattice wave speeds. This ratio is very sensitive to the lattice parameter κ (ratio of the particle separation to the screening length) in a very useful range of $\kappa \lesssim 2$. It was found that only a two-dimensional lattice model can provide a quantitative description of the vertical waves, while a linear chain model gives only a qualitative agreement.

DOI: 10.1103/PhysRevE.71.026410 PACS number(s): 52.27.Lw, 52.35.Fp, 46.40.−f, 62.30.+d

I. INTRODUCTION

Complex (dusty) plasmas [1–5] consist of micron sized grains immersed in an ion-electron plasma. Grains charge up and interact collectively producing a wide range of interesting effects. They can be easily observed in real time with a video camera and therefore the kinetics of individual grains can be studied. Complex plasmas exist in gaseous (weakly coupled), liquid, or solid (strongly coupled) phase states.

Strongly coupled complex plasmas (plasma crystals) were predicted [6] and observed experimentally [7–10] only recently. They can be used as macroscopic model systems of liquids and solids to observe phase transitions [6,7], shocks [11–15], solitons [16,17], and various wave modes.

A plasma crystal, like any elastic solid, can sustain longitudinal (compressional) and transverse (shear) wave modes [18]. Dispersion relations of a two-dimensional hexagonal grid of charged particles interacting via Yukawa potential were obtained along the irreducible element of the first Brillouin zone in Ref. [19]. Even though these calculations were performed for typically overdamped colloidal crystals, they neglected friction. In plasma crystals the friction due to the gas drag is four to five orders of magnitude lower, hence the result of Ref. [19] is expected to apply to these systems much better. Compressional waves in plasma crystals were observed experimentally in Refs. [20–22] and transverse waves were observed in Ref. [23]. Dispersion relations of these wave modes were measured in Ref. [24] for long wavelengths. Using naturally excited or thermal waves it became possible to measure the dispersion relations even for very short wavelength waves [25], as well as their dependence on the direction of propagation [26].

There is one more wave mode in two-dimensional (2D) elastic solids due to the fact that they exist in a 3D space, the so called vertical transverse mode. If a 2D membrane is placed horizontally then out of plane (vertical) motion produces this mode. The vertical transverse mode was studied theoretically in Refs. [27,28]. It was found that it has inverse optical-like dispersion. Self-excited vertical oscillations were observed experimentally [29] and explained by an instability of the vertical transverse mode. A dispersion relation of the vertical transverse waves was obtained using a molecular dynamics simulation [30]. Transverse waves were observed experimentally in a one-dimensional Yukawa chain [31].

Wave packets were intensively studied in optics [32,33], in atomic beams [33,34], and in plasmas [35]. Numerous applications include optical and radio communications, metrology, and atomic lithography.

Propagation of wave packets is usually observed to study how the wave energy is transferred. In the approximation of small dispersion and nonabsorbing medium, the speed of energy transfer is equal to the group velocity of the medium. In case of strong dispersion and absorption [36,37], however, the shape of the wave packet changes significantly as it propagates, and its speed is not determined only by the dispersion properties of the medium. It was pointed out in Ref. [36] that the group velocity, the energy transport velocity, and the signal velocity are not equal to each other in general case.

The wave packet propagation was studied experimentally and theoretically using different approximations in various dispersive media [38], optical fibers [32], and cold plasmas [35]. It was demonstrated experimentally that the wave packet velocity could be different from the wave group velocity [35].

Here we report an experimental observation of a vertical transverse wave packet with constant width, propagating in a monolayer hexagonal plasma crystal. We analyze theoretically how the medium dispersion, inhomogeneity, and dissipation affect the width of the wave packet observed in the experiment.

*Permanent address: Moscow Engineering and Physics Institute, Kashirskoe shosse 31, 115409 Moscow, Russia.

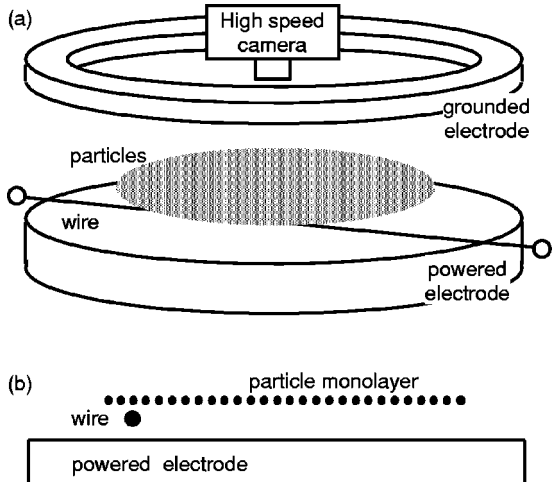

FIG. 1. Sketch of the apparatus. (a) Oblique view. Spherical monodisperse particles are charged negatively and form a monolayer, levitating in the plasma sheath above the lower electrode. (b) Side view. The grounded wire is placed below the particles. Short negative pulses applied to the wire excite vertical wave packets.

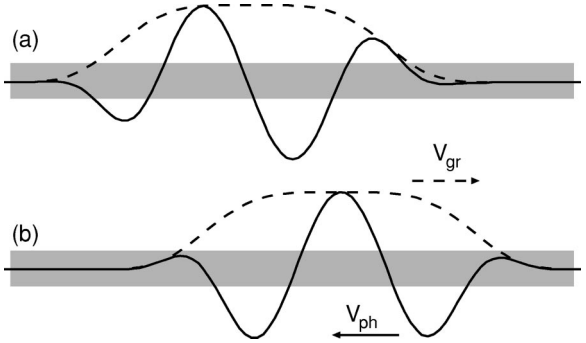

FIG. 2. Side view of the vertical wave packet propagating in a monolayer lattice. (a) Initial position of the packet. (b) Displaced packet. The group velocity V_{gr} (the velocity of the packet envelope marked by the dashed line) is directed right, while the phase velocity V_{ph} (the velocity of the modulating wave marked by the solid line) points left. The illuminating laser beam is indicated by the gray bar. We observe only the areas where it intersects the lattice (solid line), which appear as moving stripes in the experiment.

II. EXPERIMENTAL SETUP AND OBSERVATIONS

The experiments were performed in a setup (Fig. 1) similar to that of Ref. [16] using a capacitively coupled radio-frequency (rf) discharge. The discharge chamber had a lower disk electrode and an upper ring electrode. The upper electrode and the chamber were grounded. A rf power of 4–10 W (measured as forward minus reverse) was applied to the lower electrode. An argon gas flow at a rate of 0.5–0.9 SCCM (SCCM denotes standard cubic centimeter per minute) maintained the working gas pressure of 1.0–1.8 Pa. Monodisperse plastic microspheres 8.9 ± 0.1 μm in diameter were levitated in the sheath above the lower electrode forming a monolayer hexagonal lattice. They were confined radially in a bowl shaped potential formed by a rim on the outer edge of the electrode. The monolayer particle cloud was about 6 cm in diameter and levitated at a height of $\simeq 9$ mm above the lower electrode. The particle number density increased about 30% from the excitation edge (Fig. 1) to the middle of the lattice and it remained approximately constant from the middle to the outer edge. The particles were illuminated by a horizontal thin (0.2–0.3 mm) sheet of light from a doubled Nd:YAG diode pumped laser (532 nm) and imaged by a top view digital video camera at 230.75 frames/s. The field of view was 1024×512 pixels or 4.42×2.21 cm and it contained about 3000 particles.

A horizontal tungsten wire 0.1 mm in diameter was placed 4 mm below the particle layer and roughly half way between the center and the edge of the electrode. The wire was normally grounded. Its height was adjusted to minimize its static influence on the particles and maximize the vertical wave excitation. The wire was placed between the plasma and the powered electrode which was self-biased at -30 V. The plasma potential was about 10 V. A short negative pulse (-25 V, 10 ms) applied to the wire 0.04 s after the start of recording pushed the particles away. Due to the lower gas pressure, shorter excitation pulse, and slightly different wire height than that used in Ref. [16], mostly vertical oscillations were excited. It was accompanied by a very weak compressional soliton (with compression ratio $\simeq 1$). A time interval of about 1 min was allowed for the lattice to come into equilibrium. Several experimental runs were recorded with very good reproducibility.

Note that using the wire excitation method we can vary neither the excitation frequency nor the wave number of the packets. The reason is that the grain interaction with the wire is long distance [39], so that all observed grains are affected with no control over the force distribution. After the voltage pulse is applied, the wave packets are formed spontaneously with very little control over the parameters. More excitation control can be obtained using laser excitation which is more local, however, it requires a more complicated setup, expensive lasers, and optics.

A side view of a propagating vertical wave packet is shown in Fig. 2. The particles forming the lattice move in the vertical direction. Due to inverse optical dispersion of the vertical waves, the packet envelope moves in one direction while the modulating waves move in the opposite direction.

The top view did not allow us to observe vertical motion of the particles directly. However, since the illuminating laser sheet is thin, grains disappear from the field of view if displaced vertically. The lattice is visible only where it is in the plane of the laser beam (Fig. 2) and the vertical waves appear as moving stripes of particles. Figure 3 shows video frames with such moving stripes. The individual particles here did not move horizontally. Note that since the displacement of the particles up or down cannot be distinguished, two identical stripes per wavelength show. This effectively doubles the apparent frequency and halves the wavelength.

The particles were illuminated by a laser sheet with a Gaussian distribution of intensity in the vertical direction with a width of 0.2–0.3 mm and therefore the particle brightness can be used to evaluate their vertical positions. When the grains were not displaced their brightness was the highest. As they moved up or down, their brightness decreased. We identified clusters of connected pixels in the video

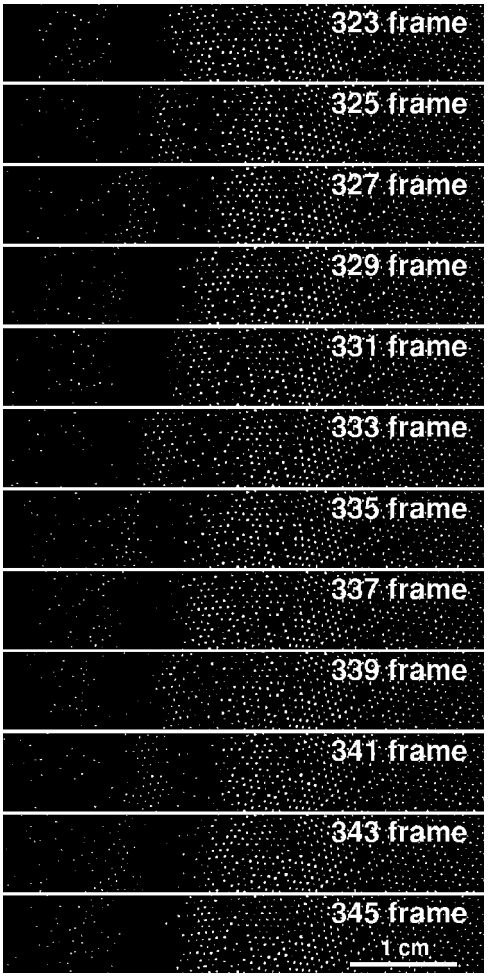

FIG. 3. Top view of the lattice at time 1.4–1.5 s after the excitation, when the wave packet was well formed. The wire positioned at the left edge of the field of view below the lattice excited the wave packet. The particles are visible only if they are in the plane of the illuminating laser sheet. The stripes of particles apparently move from right to left due to the vertical wave motion. They correspond to the lines of constant phase (phase motion). Individual particles do not move horizontally. The numbers on the images indicate the frame number (at 230.75 fps).

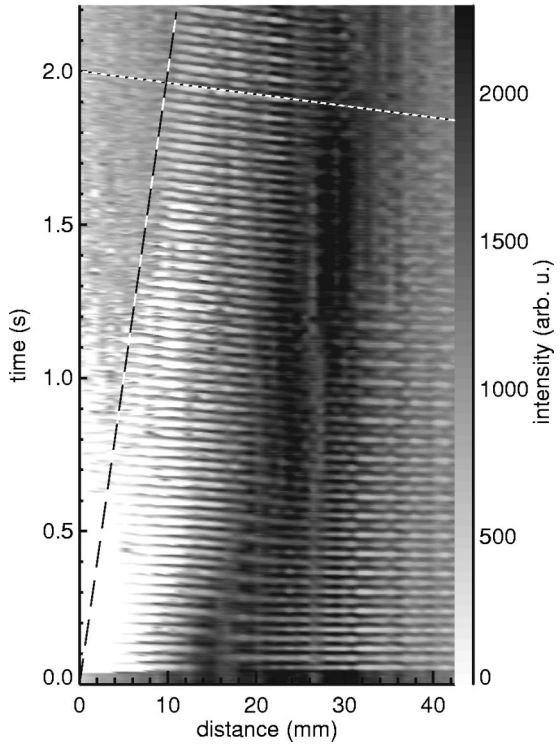

FIG. 4. Visualization of an experimentally observed vertical wave packet. The intensity of light scattered by the particles (which depends on their vertical positions) is plotted vs distance and time. Lighter regions indicate where particles are displaced from their equilibrium positions. Vertical oscillations with a frequency of about 16 Hz are excited by an electrostatic pulse applied to a wire placed at distance 0 mm. A wave packet, appearing as inclined stripes, is formed at time 1 s. The dashed line is drawn approximately through the ends of the stripes. Its angle indicates the packet group velocity of 4.5 mm/s. The dotted line is drawn parallel to the stripes. It shows the vertical wave phase velocity of -290 mm/s, which is negative because the dispersion relation is inverse optical like.

frames and summed their pixel values, so that both the particle visible size and its brightness were taken into account. The values obtained were then averaged in narrow bins parallel to the wire in order to reduce random fluctuations. These values were plotted as a grayscale map versus distance and time in Fig. 4 (see also experiment 1 in Table I for the conditions).

Figure 4 shows a visualization of a vertical wave packet propagating from the excitation source positioned at 0 mm. The data were taken for the rf power of 4 W, and gas pressure of 1.0 Pa (experiment 1 in Table I). Initially horizontal stripes indicate stationary lattice oscillations. At 1 s the oscillations start propagating, i.e., the stripes become inclined (Fig. 4) and move away from the right edge of the graph. At this time the wave packet is formed. Its group velocity $V_{gr}=4\pm1$ mm/s, its phase velocity $V_{ph}=-290\pm20$ mm/s, and its wavelength $\lambda=18$ mm. The phase velocity is negative due to inverse optical-like dispersion of the vertical wave mode. Inverse or negative dispersion means that the wave frequency ω decreases with increasing wave number k. Optical-like dispersion means that $\omega\neq0$ at $k=0$ or that there are some nonpropagating oscillations. The amplitude of the vertical motion decreases due to neutral gas damping. The resonance frequency of the vertical oscillations $\Omega_v=16$ Hz was measured in a separate experiment under the same conditions. The dust-lattice wave velocity $c_{DL}=35\pm2$ mm/s was measured as the speed of small compressional ripples using the method of Ref. [16].

We repeated the experiment at the rf power of 10 W and the gas pressure of 1.8 Pa (experiment 2 in Table I). We could excite the vertical wave packets, however, due to higher pressure, they were damped quicker. The measurements of the group speed were less precise. We obtained $V_{gr}=2.5\pm1$ mm/s, $V_{ph}=-300\pm20$ mm/s, $c_{DL}=30\pm2$ mm/s.

TABLE I. Experimental conditions and measured parameters.

Experiment	Power (W)	Pressure (Pa)	Ω_v (Hz)	V_{ph} (mm/s)	V_{gr} (mm/s)	C_{DL} (mm/s)	λ(mm)	a (mm)	R	κ
1	4	1.0	16	-290 ± 20	4 ± 1	35 ± 2	18 ± 2	0.70	$0.97\pm15\%$	0.75
2	10	1.8	21	-300 ± 20	2.5 ± 1	30 ± 2	30 ± 3	0.54	$0.9\pm18\%$	0.85

III. THEORY

A. Theoretical model

The *theoretical model* is based on the 3D equations of lattice motion:

$$m\ddot{\mathbf{r}}_s = \mathbf{f}_s^{fr} + \mathbf{f}_s^{v} + \mathbf{f}_s^{int}, \quad \mathbf{f}_s^{fr} = -m\nu\dot{\mathbf{r}}_s,$$

$$\mathbf{f}_s^{v} = -\nabla P, \quad P = [\Omega_v^2 z_s^2 + \Omega_h^2(x_s^2 + y_s^2)]/2,$$

$$\mathbf{f}_s^{int} = -\nabla U_s, \quad U_s = Q^2 \sum_{j\neq s} r_{sj}^{-1} \exp(-r_{sj}/\lambda_D), \tag{1}$$

where m is the mass of the particles, $\mathbf{r}=(x,y,z)$ is the particle coordinate with the subscripts s and j denoting different particles, $\mathbf{f}_s^{fr}$ is the friction due to collisions with neutrals (Epstein drag), $\mathbf{f}_s^{v}$ is the vertical confinement force due to a parabolic potential P with vertical (Ω_v) and horizontal (Ω_h) eigenfrequencies, $\mathbf{f}_s^{int}$ is the grain-grain interaction force, ν is the neutral (Epstein) damping rate, U_s is the grain-grain interaction screened Coulomb (Yukawa) potential energy, Q is the particle charge, $r_{sj}=|\mathbf{r}_s-\mathbf{r}_j|$ is the intergrain distance, and λ_D is the screening length.

The particles are confined more strongly in the vertical direction than in the horizontal ($\Omega_v \gg \Omega_h$). If we consider only a small part of the lattice in the middle of the potential well, then the horizontal confinement can be neglected. This is equivalent to an infinite lattice confined vertically. In general the vertical confinement potential is not parabolic [40], however, for vertical oscillations of very small amplitude we can neglect the nonquadratic terms.

Equations (1) are solved using perturbation theory. We linearize them by introducing $\mathbf{r}_s=\mathbf{R}_s+\delta\mathbf{r}_s$, where $\delta\mathbf{r}_s$ is a small deviation from the static equilibrium position of the particle $\mathbf{R}_s$. In addition to the well known longitudinal and transverse modes (calculated for a monolayer hexagonal lattice in Ref. [26]) we obtain a vertical transverse wave mode:

$$z_{tt} + \nu z_t = -\Omega_v^2 z - c_v^2 z_{xx}. \tag{2}$$

Here, $z=z(x,t)$ is the vertical particle displacement (with respect to the equilibrium position), c_v is the characteristic speed of the vertical wave mode defined by the elastic properties of the crystal.

B. Dispersion properties of the vertical transverse waves

We solve Eq. (2) assuming small amplitude harmonic motion $\delta\mathbf{r}_s=\vec{\xi}_{\mathbf{k},\omega}\exp(i\mathbf{k}\cdot R_s - i\omega t)$. The dispersion relation (in the long-wavelength approximation) has the form

$$\omega^2 = \Omega_v^2 - k^2 c_v^2. \tag{3}$$

c_v can be calculated taking into account the particular arrangement of the particles in the lattice. Using a speed parameter $c_*=Q/\sqrt{ma}$ (where a is the particle separation), and a screening parameter $\kappa=a/\lambda_D$, we calculate the characteristic speed of the vertical wave mode for a monolayer hexagonally symmetric lattice:

$$c_v = c_* f_{vert}^{(2D)}(\kappa), \quad f_{vert}^{(2D)}(\kappa) = \left[\frac{\kappa}{4}\sum_{n,m=-\infty}^{+\infty}\frac{1+R_{nm}}{R_{nm}}e^{-R_{nm}}\right]^{1/2}, \tag{4}$$

where $R_{nm}=\kappa\sqrt{n^2+m^2+mn}$, indices (n,m) denote the particle position in the lattice, and the term at $n=m=0$ is excluded. For a 1D case (linear chain) the characteristic speed of the vertical wave mode is

$$c_v = c_* f_{vert}^{(1D)}(\kappa), \quad f_{vert}^{(1D)}(\kappa) = \left[\sum_{n=1}^{\infty}\frac{1+n\kappa}{n}e^{-n\kappa}\right]^{1/2}, \tag{5}$$

which has an analytical solution:

$$f_{vert}^{(1D)}(\kappa) = \left[\frac{\kappa e^{\kappa}}{e^{\kappa}-1} - \ln(e^{\kappa}-1)\right]^{1/2}. \tag{6}$$

Figure 5 shows how the characteristic speed of the vertical wave mode depends on the screening parameter. The result is qualitatively the same for both chain (1D) and lattice (2D) models, however, quantitatively the characteristic speeds are different by a factor 1.5 at $\kappa=1$ and 2 at $\kappa=0.5$. This means that the linear chain model provides only a rough

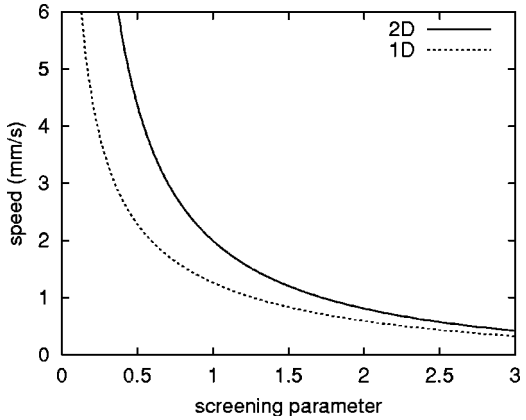

FIG. 5. Vertical characteristic speed c_v vs screening parameter κ analytically calculated for a two-dimensional hexagonal lattice (solid line) and a linear chain (dotted line). The discrepancy between the two models is very significant at $\kappa \lesssim 2$.

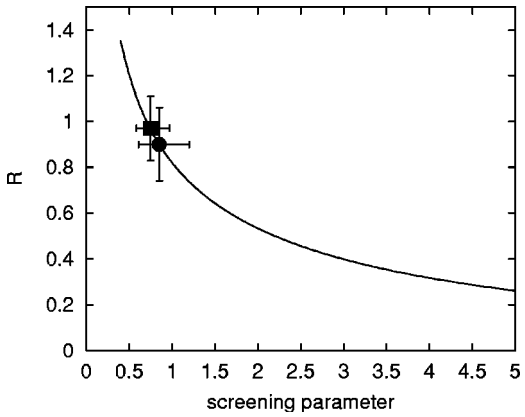

FIG. 6. Ratio $R(\kappa)$ (solid line) of the vertical c_v and compressional c_{DL} characteristic speeds vs screening parameter κ analytically calculated for a two-dimensional hexagonal lattice. It is a strong function of κ and therefore can be used for complex plasma diagnostics to determine the screening length. The filled square and the filled circle indicate R measured in the experiments 1 and 2 (Table I), respectively. κ is then reconstructed using the known inverse dependence $\kappa(R)$.

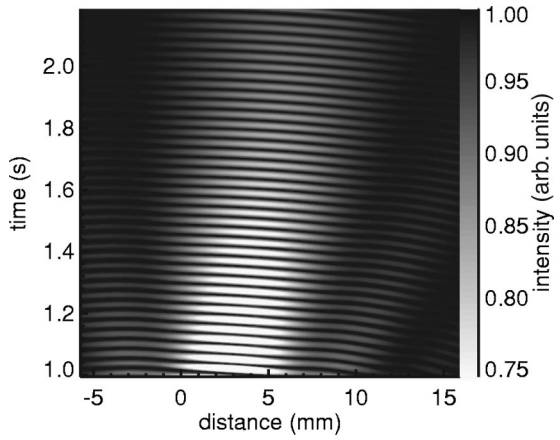

FIG. 7. Visualization of an analytically calculated wave packet propagating in a dispersive medium vs distance and time. The gray-scale map simulates the lattice illuminated by a laser sheet (similar to the experimental observation), with lighter regions indicating where particles are displaced in the vertical direction from their equilibrium position. The wave packet spreads due to dispersion (its half-amplitude width increases). However, since the wave amplitude also decreases with time due to neutral damping, the visible packet width (determined by a visibility threshold) remains nearly constant.

qualitative description of the hexagonal lattice.

The vertical wave dispersion relation (3) implies that the phase V_{ph} and group V_{gr} velocities should obey the relation

$$-V_{ph}V_{gr}=c_v^2, \tag{7}$$

and therefore they always have opposite signs. Physically this means that while a modulated wave packet moves in one direction, the individual waves inside it move in the other direction. This is the well known backward wave, observed earlier in a linear chain [41] and in systems with an inverse optical-like dispersion.

Note that Eq. (7) has a very simple geometric interpretation. Let us introduce two new variables ϑ and θ such that $V_{ph}=c_v \tan\theta<0$, $V_{gr}=c_v \tan\vartheta>0$, then Eq. (7) can be rewritten as $\tan\theta \tan\vartheta=-1$. This is equivalent to $\cos(\theta-\vartheta)=0$, or $\theta-\vartheta=\pi/2$. This means that if Fig. 4 is presented using (x,c_vt) coordinates with the same unit length, the lines representing the group and phase velocity (dashed and dotted lines, respectively) are perpendicular to each other.

For long wavelengths, the second term on the right hand side of Eq. (3) can be treated as a small correction. Then we have approximately

$$\omega \simeq \Omega_v - \frac{k^2c_v^2}{2\Omega_v}, \quad V_{ph} \simeq -\frac{\Omega_v}{|k|}<0, \quad V_{gr} \simeq \frac{c_v^2|k|}{\Omega_v}>0, \tag{8}$$

assuming that $k=-|k|<0$ to fit the experiment (Fig. 4).

C. Screening length diagnostic method

Equations (4) and (5) have the same form as Eq. (3) of Ref. [42] for the characteristic speed of a small compressional perturbation:

$$c_{DL}=c_* f_{DL}(\kappa), \tag{9}$$

where c_{DL} is the dust-lattice (compressional) wave speed, and f_{DL} is a function of κ. It turns out that the functions $f_{DL}(\kappa)$ and $f_{vert}(\kappa)$ have very different κ dependencies. The ratio of the vertical/compressional wave speeds is

$$R(\kappa)=\frac{c_v}{c_{DL}}=\frac{f_{vert}^{(2D)}(\kappa)}{f_{DL}(\kappa)}. \tag{10}$$

The function $R(\kappa)$ depends strongly on the screening parameter (Fig. 6) in the most useful range of $0.5<\kappa<2$, but not on particle charge. Combining Eqs. (10) and (7) one can find that

$$R(\kappa)=\frac{\sqrt{-V_{ph}V_{gr}}}{c_{DL}}. \tag{11}$$

Using the values of V_{ph}, V_{gr}, and c_{DL} measured in the experiment we find the values of R. Then κ is calculated from Eq. (10). We find that $R=0.97\pm15\%$ and therefore $\kappa=0.75$ (filled square in Fig. 6) at the experimental conditions of Fig. 4 (experiment 1 in Table I). Another experiment (experiment 2 in Table I), performed at 10 W rf power (filled circle in Fig. 6) produced $R=0.9\pm18\%$ and therefore $\kappa=0.85$. The measured values of κ are somewhat lower than the expected value of 1–1.2 most likely because this calculation did not take into account lattice inhomogeneity.

D. Wave packet in a dispersive medium

We find an analytical solution for a wave packet propagating in a dispersive medium. Suppose that Eq. (2) has a solution:

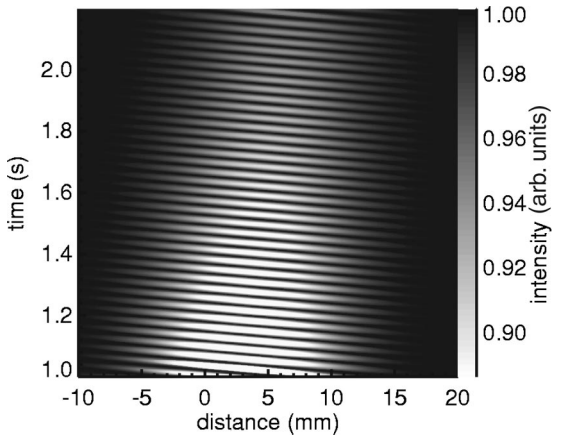

FIG. 8. Visualization of an analytically calculated wave packet propagating in an inhomogeneous medium vs distance and time. The grayscale map simulates the lattice illuminated by a laser sheet (similar to the experimental observation), with lighter regions indicating where particles are displaced in the vertical direction from their equilibrium position. The width of the wave packet decreases due to the inhomogeneity of the lattice.

$$z = [A(x,t)e^{i\Omega_v t} + A^*(x,t)e^{-i\Omega_v t}]e^{-\nu t/2}, \tag{12}$$

where we separate the fast oscillating part $e^{i\Omega_v t}$ and the wave amplitude $A(x,t)$ (A^* is its complex conjugate) which is slowly varying in space and time due to dispersion. Substituting Eq. (12) into Eq. (2) and omitting all higher order terms, we obtain a simplified equation for the wave amplitude:

$$iA_t + \left[\frac{c_v^2}{2\Omega_v}\right]A_{xx} = 0. \tag{13}$$

This equation is formally equivalent to the Schrödinger equation describing the wave function of a force-free quantum system. If we multiply Eq. (13) by the Planck constant $\hbar$, identify the wave amplitude A with the wave function Ψ, and introduce a "quasiparticle mass" $M=\hbar\Omega_v/c_v^2$, the analogy will be complete. This analogy shows that a compact pulse spreads as it propagates. At a time scale $\sim t$ the pulse width L increases by $\Delta L=\sqrt{2c_v^2 t/\Omega_v}$. In our experiment the propagation time is $t=2.2$ s, so that $\Delta L=7$ mm.

Equations (12) and (13) have a particular solution:

$$z(x,t) = A_0 e^{-\nu t/2}\int_{\xi_-}^{\xi_+} d\eta \cos(\eta^2 + \omega t + kx),$$

$$\xi_\pm = \frac{x \pm L - V_{gr}t}{\sqrt{2Dt}}, \quad \omega = \Omega_v - \frac{k^2 c_v^2}{2\Omega_v}, \quad D = \frac{c_v^2}{\Omega_v}, \tag{14}$$

which describes propagation of a sinusoidally modulated wave pulse with rectangular initial shape (Fig. 7). Dispersion causes the wave packet to spread.

Damping reduces the apparent width of the pulse and thus visibly counteracts the dispersion. As the packet amplitude decreases due to damping, the part of the packet with the vertical displacement larger than the width of the illuminating laser sheet becomes smaller. This is equivalent to change of the detection threshold. Therefore even a constant width pulse with reducing amplitude will appear more narrow.

E. Wave packet in an inhomogeneous medium

Medium inhomogeneity is a mechanism that reduces the real (half amplitude) wave packet width. The lattice we used in the experiment was slightly inhomogeneous with the particle separation decreasing by 10% from the excitation edge to the middle. In order to take inhomogeneity into account we assume that the vertical resonance frequency Ω_v in Eq. (2) depends on the coordinate $\Omega_v=\Omega_v(x)$ or

$$\Omega_v^2(x) = \Omega_0^2\left(1 - \epsilon^2\frac{x^2}{L_{cr}^2}\right), \tag{15}$$

where Ω_0 is the resonance frequency in the center of the lattice, L_{cr} is the half size of the lattice, and $\epsilon \ll 1$ is a parameter that characterizes the inhomogeneity. The corresponding inhomogeneity length is $L_{inh}=L_{cr}/\epsilon \gg L_{cr}$.

Treating dispersion and inhomogeneity as small corrections, and assuming that the solution takes the form of Eq. (12), we find a generalized Eq. (13) in the case of a weakly inhomogeneous medium:

$$iA_t + \left[\frac{c_v^2}{2\Omega_0}\right]A_{xx} - \frac{\epsilon^2\Omega_0}{2L_{cr}^2}x^2 A = 0, \quad |x| < L_{cr}. \tag{16}$$

This equation is known to have localized solutions. Let us consider the following function as a possible solution:

$$A(x,t) = A_0 \exp\left(i\beta(t) + ikx - \frac{[x-\alpha(t)]^2}{2L^2}\right), \tag{17}$$

where $\beta(t)$ and $a(t)$ are time-dependent functions, and k and L are constants. In the case $\epsilon \ll 1$ the solution can be written in the form

$$z(x,t) = A_0 \exp\left(-\frac{\nu t}{2} + i\beta(t) + ikx - \frac{[x-a(t)]^2}{2L^2}\right),$$

$$\dot{\beta} = \Omega_0 - \frac{k^2 c_v^2}{2\Omega_0} + O(\epsilon), \quad \dot{a} = \frac{kc_v^2}{\Omega_0} + O(\epsilon), \quad L = \sqrt{\frac{c_v L_{cr}}{\epsilon\Omega_0}}, \tag{18}$$

where the small corrections $O(\epsilon)$ can be neglected. This solution is valid for a time scale

$$\Delta t \ll \frac{2\pi L_{cr}}{\epsilon c_v}. \tag{19}$$

The visualization of the wave packet corresponding to Eq. (18) is shown in Fig. 8. The parameters Ω_0, λ, V_{gr}, and V_{ph} were chosen the same as in the experiment, and it was assumed that $L_{cr}=30$ mm, and $\epsilon=0.2$. The time limit $\Delta t \simeq 33$ s of Eq. (19) is therefore satisfied. The wave packet is focused due to the lattice inhomogeneity.

IV. SUMMARY

Nonspreading vertical wave packets were excited in a hexagonal monolayer plasma crystal, and their propagation

was observed. It was found that the phase velocity exceeded the group velocity by a factor 65 and was directed in the opposite direction as expected for an inverse optical-like dispersion relation. A theory based on the three-dimensional equations of motion was developed to explain why the wave packets propagate keeping their width constant. It was found that while dispersion causes the wave packet to spread, lattice inhomogeneity focuses it. Neutral gas damping can visually counteract spreading. The theory uses a long-wavelength weak dispersion weak inhomogeneity approximation. It describes well formed vertical wave packets (not the initial stage after the excitation pulse is applied) and shows good agreement with the experiment. The experimental (Fig. 4) and theoretical (Figs. 7 and 8) results are presented in a similar graphical form to facilitate their direct comparison, which shows very good agreement.

A plasma diagnostic method was developed which is based on the ratio between vertical and dust-lattice waves speeds. This ratio is very sensitive to the screening parameter in the very useful range of $\kappa \lesssim 2$. It was verified that for this range of screening parameters only a monolayer lattice model can provide a quantitative description of the vertical waves, while a linear chain model gives us only a qualitative description.

ACKNOWLEDGMENTS

We thank R. Quinn and A. Ivlev for useful discussions.

[1] E. Whipple, T. Northrop, and D. Mendis, J. Geophys. Res. **90**, 7405 (1985).
[2] C. K. Goertz, Rev. Geophys. **27**, 271 (1989).
[3] T. Northrop, Phys. Scr. **45**, 475 (1992).
[4] V. Tsytovich, Usp. Fiz. Nauk **167**, 57 (1997) [Phys. Usp. **40**, 53 (1997)].
[5] V. Fortov, A. Khrapak, V. Molotkov, O. Petrov, and S. Khrapak, Usp. Fiz. Nauk **174**, 495 (2004) [Phys. Usp. **47**, 447 (2004).
[6] H. Ikezi, Phys. Fluids **29**, 1764 (1986).
[7] H. Thomas, G. Morfill, V. Demmel, J. Goree, B. Feuerbacher, and D. Möhlmann, Phys. Rev. Lett. **73**(5), 652 (1994).
[8] Y. Hayashi and K. Tachibana, Jpn. J. Appl. Phys., Part 2 **33**, L804 (1994).
[9] J. Chu and I. Lin, Physica A **205**, 183 (1994).
[10] J. Chu and I. Lin, Phys. Rev. Lett. **72**, 4009 (1994).
[11] D. Samsonov, J. Goree, Z. W. Ma, A. Bhattacharjee, H. M. Thomas, and G. E. Morfill, Phys. Rev. Lett. **83**, 3649 (1999).
[12] D. Samsonov, J. Goree, H. M. Thomas, and G. E. Morfill, Phys. Rev. E **61**, 5557 (2000).
[13] D. Samsonov, G. Morfill, H. Thomas, T. Hagl, H. Rothermel, V. Fortov, A. Lipaev, V. Molotkov, A. Nefedov, O. Petrov, A. Ivanov, and S. Krikalev, Phys. Rev. E **67**, 036404 (2003).
[14] F. Li and O. Havnes, Phys. Rev. E **64**, 066407 (2001).
[15] J. E. Hammerberg, T. C. Germann, and B. L. Holian, in *Shock Compression of Condensed Matter*, edited by Michael D. Furnish, Yasuyuki Horie, and Naresh N. Thadhani, AIP Conf. Proc. No. 620 (AIP, Melville, NY, 2002), p. 359.
[16] D. Samsonov, A. Ivlev, R. Quinn, G. Morfill, and S. Zhdanov, Phys. Rev. Lett. **88**, 095004 (2002).
[17] S. K. Zhdanov, D. Samsonov, and G. E. Morfill, Phys. Rev. E **66**, 026411 (2002).
[18] L. Landau and E. Lifshitz, *Theory of Elasticity* (Pergamon, Oxford, 1970).
[19] F. Peeters and X. Wu, Phys. Rev. A **35**, 3109 (1987).
[20] M. Zuzic, H. Thomas, and G. Morfill, J. Vac. Sci. Technol. A **14**, 496 (1996).
[21] J. Pieper and J. Goree, Phys. Rev. Lett. **77**, 3137 (1996).
[22] A. Homann, A. Melzer, R. Madani, and A. Piel, Phys. Lett. A **173**, 242 (1998).
[23] S. Nunomura, D. Samsonov, and J. Goree, Phys. Rev. Lett. **84**, 5141 (2000).
[24] S. Nunomura, J. Goree, S. Hu, X. Wang, and A. Bhattacharjee, Phys. Rev. E **65**, 066402 (2002).
[25] S. Nunomura, J. Goree, S. Hu, X. Wang, A. Bhattacharjee, and K. Avinash, Phys. Rev. E **89**, 035001 (2002).
[26] S. Zhdanov, S. Nunomura, D. Samsonov, and G. Morfill, Phys. Rev. E **68**, 035401 (2003).
[27] S. V. Vladimirov, P. V. Shevchenko, and N. F. Cramer, Phys. Rev. E **56**, R74 (1997).
[28] A. V. Ivlev and G. Morfill, Phys. Rev. E **63**, 016409 (2001).
[29] S. Takamura, T. Misawa, N. Ohno, S. Nunomura, M. Sawai, K. Asano, and P. K. Kaw, Phys. Plasmas **8**, 1886 (2001).
[30] K. Qiao and T. W. Hyde, Phys. Rev. E **68**, 046403 (2003).
[31] B. Liu, K. Avinash, and J. Goree, Phys. Rev. Lett. **91**, 255003 (2003).
[32] D. Anderson and M. Lisak, Phys. Rev. A **35**, 184 (1987).
[33] A. Valencia, M. Chekhlova, A. Trifonov, and Y. Shih, Phys. Rev. Lett. **88**, 183601 (2002).
[34] F. Buchkremer, R. Dumke, H. Levsen, G. Birkl, and W. Ertmer, Phys. Rev. Lett. **85**, 3121 (2000).
[35] Y. Amagishi, H. Nakagawa, and M. Tanaka, Phys. Rev. E **50**, 2217 (1994).
[36] L. Brillouin, *Wave Propagation and Group Velocity* (Academic, New York, 1960).
[37] T. Havelock, The *Propagation of Disturbances in Dispersive Media* (Stechert-Hafner, New York and London, 1964).
[38] B. Nodland, Phys. Rev. E **55**, 3647 (1997).
[39] D. Samsonov, A. Ivlev, G. Morfill, and J. Goree, Phys. Rev. E **63**, 025401 (2001).
[40] A. V. Ivlev, R. Stterlin, V. Steinberg, M. Zuzic, and G. Morfill, Phys. Rev. Lett. **85**, 4060 (2000).
[41] T. Misawa, N. Ohno, K. Asano, M. Sawai, S. Takamura, and P. Kaw, Phys. Rev. Lett. **86**, 1219 (2001).
[42] S. Zhdanov, R. Quinn, D. Samsonov, and G. E. Morfill, New J. Phys. **5**, 74 (2003).